Final technical report

USGS Award Number: G15AP00048
Title of award: Earthquake Hazard Assessment of the Winter Rim fault system, Eastern Oregon
Author: Anne E. Egger
Central Washington University
400 E. University Way
Ellensburg, WA 98926-7418
509-963-2870
annegger@geology.cwu.edu

Term covered by the award: June 16, 2015—Sept. 30, 2016

Abstract

The Winter Rim fault system in Eastern Oregon marks both the northern and western extent of significant Basin and Range faulting. The fault system comprises two segments with Holocene fault scarps: the Winter Ridge and Slide Mountain segments, which are roughly orthogonal to each other. In addition, the Summer Lake basin hosts the Ana River fault, synthetic to the Winter Ridge fault, and the Thousand Springs (or Summer Lake) fault, which is antithetic to the Winter Ridge fault. All four fault segments cut and offset Quaternary sediments, but none have historic surface ruptures.

Topographic profiles indicate that the Winter Ridge segment has accumulated approximately twice as much vertical offset as the Slide Mountain segment. In addition, the Thousand Springs fault appears to act independently of the Winter Rim system – it runs the length of the basin and magnitude calculations are consistent with a length of ~30 km and a mean displacement of 2.0 m. Comparison of paleoseismic studies with new radiocarbon dates on paleolake-level changes suggest that earthquake recurrence intervals have varied significantly over the last 80 ka, with shorter recurrence intervals associated with rapid changes in pluvial lake levels.

In combination, these results suggest that current slip rates and recurrence intervals underestimate the rupture potential and seismic hazard of faults in the Summer Lake basin.

INTRODUCTION

Tectonic setting and earthquakes of the northwestern Basin and Range

The northwestern Basin and Range (NWBR) of south-central Oregon, northeastern California, and northwestern Nevada, lies north of the Mendocino triple junction and thus inboard of the Cascadia subduction zone (Figure 1). The current phase of extension began in this region ca. 12 Ma; since then, approximately 5-15% bulk extension has occurred (Egger and Miller, 2011; Scarberry et al., 2010; Treerotchananon, 2009), primarily along a few N- to NNE-trending normal faults that decrease in offset and die out northwards (Figure 2). A pervasive, NNW-trending structural fabric is also apparent throughout the region (Figure 2). This fabric appears to accommodate a minor component of NE-directed extensional deformation (Pezzopane and Weldon, 1993; Trench et al., 2012) and facilitates step-overs in both range-bounding normal faults such as the Abert Rim fault (Scarberry et al., 2010) and minor faults in the Larkspur Hills (Strickley, 2014) and elsewhere.

The region is tectonically active (Berg and Baker, 1963; Bryant, 1990; Uhrhammer, 1991): though no large earthquakes have occurred historically, Holocene and latest Pleistocene fault scarps line many of the range-fronts (Figure 2). Due to the remoteness of the region and the low population, few paleoseisemic studies have been undertaken; the locations of known paleoseismic trenches are shown in Figures 2 and 3. Trenching along the Surprise Valley fault (Figure 2) reveals five surface-rupturing earthquakes in the last 20 ka, with the most recent earthquake occurring 1.2 ± 0.1 ka (Personius et al., 2009). In the Summer Lake basin (Figure 2), a trench along the E-W-oriented Slide Mountain fault may indicate three surface-rupturing events prior to 2130 ± 90 yr and most likely while the most recent pluvial Lake Chewaucan was

present (Pezzopane, 1993). At the north end of the basin on the Ana River fault, several trenches reveal three earthquakes since ca. 15 ka, but only four in the 70 ky prior (Langridge et al., 2001; Weldon et al., 2009). All of these investigations share similar conclusions: that slip rates and earthquake recurrence intervals along these faults have varied over the late Pleistocene and the Holocene. These results fit with other studies around the Basin and Range that note slip rate variations along the Wasatch Fault at different time scales (Friedrich et al., 2003) and other evidence for "grouping and migration" of fault slip events (Wallace, 1987). Variability in slip rates makes hazard assessment more challenging, as it requires a longer record of earthquakes and measurable offset along faults to constrain the amount of variability.

Recent earthquake activity in the NWBR appears to be dominated by swarms, as originally described by Mogi (1963): a sequence of shocks, generally $M_w<5$, that increases in frequency gradually and then declines, without a single main shock of larger magnitude. Historical events include a 1968 swarm in the Warner Valley (Schaff, 1976), a 1974 swarm near Denio, Nevada (Richins, 1974), a possible swarm near Lakeview, OR, in 1923 (Berg and Baker, 1963) and a more recent one in 2004 (Richardson et al., 2010), and the 2014-15 Sheldon swarm in northwestern Nevada (Wolterbeek, 2015) (Figure 2). Earthquake swarms have been attributed to heterogeneous crustal structure (Mogi, 1963) and are commonly interpreted to be associated with fluid injection in the subsurface, including magma and geothermal fluids (Smith and Sbar, 1974). Others have suggested they occur primarily in regions of crustal extension, particularly releasing bends of major strike-slip faults (Weaver and Hill, 1978), are associated with aseismic creep (Llenos et al., 2009; Lohman and McGuire, 2007), or some combination (Vidale and Shearer, 2006). A common characteristic of the NWBR swarms is that they do not map along the range-

front faults. Instead, they occur at shallow depths (<12 km) beneath areas of higher elevation (Figure 2). Because earthquake swarms generally do not include any earthquakes with M_w>5, they are unlikely to leave a surface rupture (e.g. Wells and Coppersmith, 1994) or any other evidence in the paleoseismic record.

In this study, we focus on the Winter Rim fault system in south-central Oregon, which includes the Ana River, Slide Mountain, and Winter Ridge fault segments (Figure 3). Existing estimates of the seismic hazard potential for the WRF system indicate a slip rate of 0.43 mm/yr, potential earthquake magnitudes of 6.5-7.2, and a recurrence interval of 3.1 ka (Crone et al., 2009). The east-dipping Winter Rim fault system bounds the west side of the Summer Lake Basin, which also hosts the west-dipping Thousand Springs (or Summer Lake) fault (Figure 3). Both of these fault systems display fault scarps that cut Quaternary sediments, but none have experienced historic surface rupturing earthquakes, nor have earthquake swarms been recorded in the immediate region. Large landslides in the basin have been interpreted to be seismogenic, however (Badger and Watters, 2004), and the fault system is undergoing active exploration for geothermal resources.

Pluvial lakes and paleoshorelines as offset markers

Throughout the Basin and Range, there is abundant evidence that valleys were filled with pluvial lakes approximately contemporaneous with glacial ages (e.g. Reheis et al., 2014, and references therein) (Figure 1 shows pluvial lake extents). Summer Lake basin is no exception, hosting pluvial Lake Chewaucan, whose maximum extent is shown in Figures 2 and 3 in relation to the surrounding region. The evidence of previous lakes serves our goals in assessing seismic

hazards. For the purposes of this study, we focus on paleoshoreline features as paleohorizontal data, which can be divided into constructional features, such as gravel bars, and erosional features, such as terraces and scarps. Here, we make use of wave-formed terraces as described by Adams and Wesnousky (1998), which are primarily erosional but can also include a thin lag deposit of gravel. Capping of wave-formed terraces by carbonate tufas is common on late Pleistocene shorelines where sediment input is low, with laminated and branching textures implying photic zone precipitation (Felton et al., 2006; McGee et al., 2012; Nelson et al., 2005). Given their association with wave-formed terraces, capping tufa samples likely record lake levels within a few meters of the lake surface, and radiocarbon dates on these tufas can be considered to record lake stillstands at those elevations. Recent studies have shown that radiocarbon tufa ages are concordant with ages derived from U-series disequilibrium analyses on the same samples, with smaller uncertainties (Ibarra et al., 2014), and that reservoir carbon (accumulation of "dead" carbon) is not a concern in these basins with no carbonate bedrock (Hudson et al., 2015).

Ages of these paleoshorelines can extend as far back as 120 ka, but can only be reliably dated using radiocarbon back to ca. 30 ka. Any given shoreline records a paleohorizontal datum when the pluvial lake was at that particular elevation. Significant deviation from that datum implies deformation that has occurred since shoreline formation. By obtaining ages for shorelines (ideally sets of shorelines) and comparing elevations of dated shorelines across major faults, we can calculate the difference in elevation and assume that this is a reasonable proxy for slip along the fault (or faults) since shoreline formation. This technique allows us to refine and correlate with slip rates obtained in other ways, such as through trenching, and potentially to extend the slip rate record further back in time.

In addition, dating paleoshorelines allows us to develop a robust lake hydrograph and compare the timing of known earthquakes with changes in lake level, which may help constrain the variability in recurrence intervals and slip rates over time. Lake Chewaucan is the pluvial lake that filled the Summer Lake basin and the adjacent Lake Abert and ZX Lake (also called the Chewaucan Marshes) (Figure 3); in this study, we focus specifically on the Summer Lake sub-basin of Lake Chewaucan (Figure 4).

METHODS

A portion of the work presented here involves compilation of data from previous studies including the age and magnitude estimates of earthquakes through paleoseismic investigations, the age and elevation of pluvial lake shorelines, and other studies that estimate timing of earthquakes. All ages are reported and discussed here as years before present (BP) to allow comparison between calibrated radiocarbon ages and other geochronologic methods, including optically stimulated luminescence (OSL) and U-series ages.

Detailed mapping and topographic analysis of fault scarps

High-resolution lidar (1 point per 0.5 m^2) data were acquired along the entire length of the Winter Rim fault system, including the Ana River fault, prior to the beginning of this grant (Figure 4). Digital elevation models (DEMs), hillshades, and slopeshades were derived from the lidar data and provided a base for detailed mapping of fault scarps and Quaternary deposits (Figure 4). Topographic profiles were drawn from the DEM across fault scarps at localities (Figure 4) where (1) no apparent sedimentation had occurred on the hanging wall post-rupture,

(2) far-field slopes were the same (or nearly so) on the hanging- and footwalls, and (3) little to no modification from construction was present. Surface offsets and vertical displacements were calculated on these profiles using standard techniques.

Radiocarbon dating of paleoshoreline tufas

We collected samples of carbonaceous paleoshoreline tufas, carbonaceous sediments, and shells from three localities on the north and east sides of the Summer Lake basin for radiocarbon dating (see Figure 4 for sample locations). Prominent shorelines on the west and south mostly do not host tufa deposits, so our sampling was necessarily spatially limited. Sample sites were restricted to *in situ* deposits on the front edge of the crest of wave-cut terraces and horizontal shoreline benches. Latitude and longitude of sample locations were recorded with a handheld GPS and elevations were derived from the lidar-based DEM or 10-m DEMs (Gesch, 2007).

Eighteen of the Summer Lake samples were selected for radiocarbon dating (Table 1) based on the (1) density of carbonate, so samples that had no to very few vesicles; (2) sample size, large enough to be handled and small enough to meet the weight criteria for shelly carbonates, and (3) prioritizing samples taken from locations where capping tufa was laterally continuous along wave-formed shorelines and in situ. Each sample was put through an ethanol wash and shaved down using a dremel with a reinforced-steel rotary saw blade to obtain 30 mg pieces of dense carbonate. In cases where the tufa was thick and laminar, all sides of the tufa were shaved until a vesicle-free core of the tufa remained to be analyzed.

Samples were analyzed by DirectAMS Radiocarbon Dating Services in Bothell, WA, according to their protocol (DirectAMS, 2015) and ages were reported to us in uncalibrated radiocarbon years. We used Calib 7.1 (Stuiver and Reimer, 1986-2015) and the IntCal13 calibration curves from Reimer et al. (2013) to calibrate our data to years before present (BP, years before 1950). Six of the eighteen samples were also run as duplicates (Table 1), particularly where initially obtained ages seemed unusually young or old.

RESULTS

Winter Ridge and Slide Mountain fault segments

Previous work

Significant fault scarps occur all along the length of Winter Ridge (Figure 4); along the southern half of the escarpment, they variably cut and are covered by massive landslides. Badger and Watters (2004) interpreted three of these landslides as seismically-triggered, requiring the combined destabilization effects of M_w 6.8–7.0 earthquakes with high groundwater conditions, suggesting that the earthquakes and landslides occurred when lake level was higher than present conditions. Badger and Watters (2004) were not able to directly date these landslides, but constrained their ages on the basis of shoreline features present (or absent) on the slides, and the amount of slip that has occurred on fault scarps post-slide. Two landslides are relatively poorly constrained to have occurred prior to the most recent highstand, but perhaps as much as several hundred ka. One, however, the Punchbowl landslide, records only the Neopluvial shoreline of Allison (1982), and thus is constrained to occur between the most recent highstand (ca. 14 ka) and 4–1.9 ka (Badger and Watters, 2004).

Pezzopane (1993) trenched the Slide Mountain fault (Figure 4) and interpreted 2–3 events prior to 2130 ± 90 yr BP and most likely 2 events since the lake highstand. He was not able to directly correlate units across the fault, however.

Topographic profiles

We measured surface offset and calculated fault slip on 53 topographic profiles across scarps along the Winter Ridge and Slide Mountain fault segments (Figure 4). Given that the two segments are roughly orthogonal in orientation to each other, and that the Winter Ridge segment is more optimally oriented to the extension direction, we considered these two segments both separately and together.

On the Winter Ridge segment, approximately 30 km long, measured scarp heights range from 1.0 m to 56.5 m with an average height of 12.2 m. Excluding the highest value of 56.5 m, significantly higher than the next highest value of 35.7 m, the average scarp height is 10.7 m. Assuming a 60° dip for the fault, fault slip ranges from 1.0 m to 47.4 m with an average slip of 11.0 m. Excluding the highest value, the next highest fault slip is 34.1 m and the average slip is 9.7 m (Figure 5).

On the Slide Mountain segment, with a length of approximately 15 km, measured scarp heights range from 1.2 m to 27.4 m with an average height of 6.0 m. Excluding the 27.4 m measurement, the next highest value is 9.7 m and the average scarp height is 5.0 m. Assuming a 60° dip for the fault, fault slip ranges from 1.1 m to 9.2 m with an average of 4.8 m (Figure 5).

Average fault slip on both segments together including all measured scarp height values is 9.8 m; excluding the two highest measurements, the average is 7.6 m.

Thousand Springs/Summer Lake fault

Previous work

This fault has virtually no previous work done on it other than identification and mapping.

Topographic profiles

Nine topographic profiles across the Thousand Springs fault yield a range of scarp heights from 0.9 m to 5.6 m, with an average of 1.9 m. Assuming a 60° fault dip, calculated fault slip ranges from 1.0 m to 6.1 m, with an average of 2.0 m (Figure 6).

Ana River Fault

Previous work

Within the Summer Lake basin, the Ana River fault (Figure 4) has been more extensively studied than either the Winter Rim or Slide Mountain faults, both because of natural exposures of the fault along the Ana River and because of the relatively low sedimentation rate in the northern part of the basin. Seven paleoseismic trenches were excavated across the fault, and natural exposures were cleaned off where the fault crosses the Ana River (Langridge, 1998; Weldon et al., 2009). The trenches and exposures revealed seven surface rupturing events in the last 80 ky, the last three of these appear to have occurred since ca. 14 ka (Egger et al., in review).

A composite stratigraphic column indicates large variability in earthquake recurrence over the last 85 ky, with three earthquakes occurring within the last 14 ky and intervals of 7-20 ka between the previous 5 earthquakes (Figure 7; Egger et al., in review).

Topographic profiles

Four topographic profiles across the Ana River fault scarp in lake sediments record fault slip of 2.6–4.6 m, with an average fault slip of 2.8 m. The scarp is only exposed over a distance of ca. 3.5 km, and nowhere along that length does it cut active deposits, suggesting that the scarp height is the result of multiple slip events, consistent with the results of trench reconstructions.

Lake Chewaucan: Summer Lake sub-basin

Previous work

Allison (1982) mapped and described geomorphic features of shorelines, dated fossils and charcoal, and connected climatic events in the basin with glacial ages. Pezzopane (2001) collected and compared topographic profiles of shorelines around Lake Chewaucan, and noted that shorelines at similar elevations differ widely in geomorphic expression and can be difficult to trace around the basin; in addition, he noted that shorelines of the same age may differ by as much as 10 m in elevation due to slip along faults within the basin.

Radiocarbon ages

Our new and compiled radiocarbon ages on shoreline tufas in the Summer Lake basin better constrain the timing of Chewaucan lake levels over the last 35 ka (Figure 7, Table 2). The

hydrograph in Figure 7 does not include all of the available radiocarbon ages for the basin, primarily because offset along faults, particularly the Ana River and Summer Lake faults (Figure 4), distorts the apparent elevation. The samples we've chosen to include in the hydrograph are those that were collected on the eastern and northeastern portions of the Summer Lake basin (Figure 4, Table 2). Notably, our youngest and highest age recorded is 13.9 ± 0.2 ka at an elevation of 1405 m near the eastern margin of the lake at Ten-Mile Ridge (Figure 4), though this may be contaminated by young carbon and may be related to a much earlier, higher highstand closer to 120 ka. The abrupt rise to the last highstand appears to have been preceded by a drop below the level of the Paisley fan, which exposes an overflow channel from the Chewaucan Marshes northwards into Summer Lake (Figure 3), as has been described by Licciardi (2001) and Allison (1982).

DISCUSSION

Earthquake magnitude estimates

Estimates of the magnitude of the most recent events along each fault were derived using two methods (Table 3). First, following the method of Wells and Coppersmith (1994) (Equation 1) and using several different surface rupture lengths (SRL) and their empirically-derived values for the constants a and b for normal-type slip:

$$\boldsymbol{M = a + b * \log(SRL)} \qquad \textit{(1)}$$

$$\boldsymbol{M = (4.86 \pm 0.34) + (1.32 \pm 0.26) * \log(SRL)}$$

The magnitude derived through Equation 1 tends to have a wide range that is not particularly useful in constraining the hazard, but it helps provide a reasonable check to see if the exposed length of the fault is reasonable.

Second, using point measurements of surface displacement from analysis of topographic profiles according to the method of Hemphill-Haley and Weldon (1999), we calculated a maximum (Equation 2) and minimum (Equation 3) limit estimate of moment magnitude (M_w). Both equations make use of the mean displacement (MD) and a set of empirically-derived combined displacement statistics (CDS) including an upper value (UVCDS), mode value (MVCDS), and lower value (LVCDS); all are based on the number of measurements and the percent of the fault sampled.

$$\boldsymbol{M_w = 6.93 + 0.82 * \log[\left(\frac{MD}{UVCDS}\right) * MVCDS]} \quad (2)$$

$$\boldsymbol{M_w = 6.93 + 0.82 * \log[\left(\frac{MD}{LVCDS}\right) * MVCDS]} \quad (3)$$

We conservatively assumed that we had sampled 75% of the fault length for the Winter Ridge segment, the Slide Mountain segment, and the two fault segments together, and also calculated as if we had sampled 100% of the same. For the Thousand Springs/Summer Lake fault, we were even more conservative and calculated magnitudes assuming we had sampled 25%, 50%, and 75% of the fault (Table 3), considering that this fault may continue as a single structure to the southeast extent of the basin (Figure 4). Since surface displacements are calculated from vertical offset based on the dip angle of the fault, we compared calculations using mean displacements (MD) assuming a 60°-dipping fault as predicted from Andersonian mechanics (Anderson, 1951).

Given that the rupture length is an estimate based on the presence of fault scarps in the youngest sedimentary units, our preferred, somewhat conservative estimate is that we have sampled 75% of the fault, and the rupture plane is dipping 60°, which suggests $\boldsymbol{M_w = 7.0–7.3}$ for the Winter Ridge-Slide Mountain fault system, and $\boldsymbol{M_w = 6.8–7.3}$ for the Thousand Springs fault. This

range more tightly constrains the estimates of M6.8–7.6 for the Winter Ridge-Slide Mountain fault from equation 1, and suggests that the earthquakes along the Thousand Springs fault may be larger than anticipated simply from the length of the fault (Table 3). This range of magnitudes is also consistent with the historic record of surface-rupturing earthquakes along segmented normal faults in the Basin and Range province (DePolo et al., 1991).

Earthquake recurrence intervals, slip rates, and hazards

Where sufficiently long earthquake records are available in the NWBR, earthquakes are not evenly distributed in space or time (Egger et al., in review). Along the Surprise Valley fault, for example, with five documented events in the last 20 ky, three earthquakes are clustered between 6–10 ka as Lake Surprise rapidly receded to modern levels. Along the Ana River fault (Figure 4), the three most recent events all occurred in the last 14 ky, with much longer intervals of 7–20 ky between the previous three events (Figure 7). Both of these apparent clusters as the lakes are receding, possibly indicating that rapid lake level change may have an influence on earthquake recurrence. This relationship is more thoroughly explored in Egger et al., in review.

This variability in earthquake recurrence intervals makes calculating slip rates and determining the seismic hazard at any particular time challenging. In addition to this inherent variability, two results of this study suggest that the slip rates and hazards are currently underestimated in the Winter Rim fault system: (1) the Winter Ridge segment has accumulated more than twice as much slip as the Slide Mountain segment (Figure 5), and (2) the Thousand Springs fault has not been included in previous hazard studies but is also capable of earthquakes with $M_w > 7$.

The current estimate of the slip rate for the Winter Rim fault system (0.43 mm/yr) is based primarily on Pezzopane (1993) and a trench across the Slide Mountain segment of the fault (Figure 4). Our results from topographic analysis of the fault scarps suggest that this slip rate could be an underestimate by a factor of two for the Winter Rim segment of the fault, assuming the two segments of the fault rupture simultaneously. Work remains to match shorelines across the basin to calculate slip rates, but these will be combined slip rates across multiple antithetic faults that are forming the Summer Lake graben, which will again result in an underestimate of the slip rate of any particular fault.

Similarly, the Thousand Springs fault has not previously been included in seismic hazard evaluations of the region, yet it has accumulated as much offset as the Ana River fault and, given its dip direction (to the W), is likely rupturing independently of the Winter Rim system. In addition, it may run the entire length of the basin (Figure 4), which suggests it is equally capable of M>7.0 earthquakes as the Winter Rim fault system.

SUMMARY

Analysis of detailed topographic profiles afforded by lidar data, in combination with comparisons to pluvial lake hydrographs, provide insight into the seismic potential of a low-strain rate normal fault such as the Winter Rim fault system. Our results suggest that current slip rates underestimate the seismic hazard in this region.

TABLE 1. LOCATION OF SAMPLES

Sample name	Latitude	Longitude	Elevation (m)
SL15AE02	**42.80892**	**-120.55169**	**1383.3**
SL15AE03	42.80836	-120.55128	1383.0
SL15AE04*	**43.05045**	**-120.68407**	**1381.2**
SL15AE05*	**43.05017**	**-120.65868**	**1343.7**
SL15AE06	**43.05006**	**-120.65854**	**1341.3**
SL15AE07	**42.83618**	**-120.61262**	**1355.4**
SL15AE08	**42.84355**	**-120.61484**	**1342.6**
SL15AE09	**42.84078**	**-120.60642**	**1350.9**
SL15JH01	**42.80892**	**-120.55169**	**1383.2**
SL15JH03	**43.01487**	**-120.75370**	**1393.6**
SL15JH04	**43.04990**	**-120.65894**	**1329.1**
SL15JH05	**43.04992**	**-120.65921**	**1328.3**
SL15JH06*	**43.04984**	**-120.65928**	**1324.9**
SL15JH07*	**42.84211**	**-120.59363**	**1407.0**
SL15JH08	**42.84228**	**-120.59378**	**1405.5**
SLT1-2C-1*	**43.02515**	**-120.70330**	**1322.4**
SLT3-1B	**43.00600**	**-120.77000**	**1316.8**
SL15BM01	42.80870	-120.55151	1383.2
SL15BM02	43.04979	-120.65844	1328.3
SL15BM03	**43.05001**	**-120.65847**	**1342.0**
SL15BM04*	**42.84256**	**-120.59393**	**1402.1**

[1] Samples for which duplicates were run

Bold samples were selected for radiocarbon geochronology

TABLE 2. RADIOCARBON AND CALIBRATED AGES

Laboratory Number	Sample ID	Material	^{14}C age (yr)	1σ	Median age (yr BP)	2σ min	2σ max	Calibrated age (ka)	2σ
AA-25320†	*unknown*	Tufa, Klippel Point	12340	90	14387	14040	14860	14.450	0.410
AA-25321†	*unknown*	Tufa, Klippel Point	12495	90	14693	14235	15101	14.668	0.433
AA-25322†	*unknown*	Tufa, Klippel Point	11910	100	13736	13540	14016	13.778	0.238
Beta-82260†	*unknown*	Tufa, Flatiron Point	11880	80	13689	13541	13872	13.707	0.166
Beta-64531†	*unknown*	Tufa, Flatiron Point	12300	80	14285	14005	14729	14.367	0.362
AA-25323†	*unknown*	Tufa, Klippel Point	12050	130	13913	13563	14247	13.905	0.342
D-AMS 013002	SL15AE02	Tufa, Loco Lake	21918	91	26118	25917	26382	**26.150**	0.233
D-AMS 013003	SL15AE04	Tufa, Flatiron Point	25859	114	30089	29643	30534	**30.089**	0.445
D-AMS 013004	SL15AE05	Tufa, Flatiron Point	12487	49	14695	14298	15034	14.666	0.368
D-AMS 013005	SL15AE06	Tufa, Flatiron Point	11565	44	13399	13296	13477	13.387	0.091
D-AMS 013006	SL15AE08	Tufa, Ten-Mile Ridge	10983	38	12828	12729	12974	12.852	0.123
D-AMS 013008	SL15JH01	Gastropod shell, Loco Lake	30371	136	34281	33975	34605	**34.290**	0.315
D-AMS 013009	SL15JH03	Tufa, W of Kilppel Point	30486	143	34456	34124	34766	**34.445**	0.321
D-AMS 013010	SL15JH05	Tufa, Johnson Creek	11873	42	13676	13572	13770	**13.671**	0.099
D-AMS 013011	SL15JH06	Tufa, Flatiron Point	22152	76	26352	26105	26621	**26.363**	0.258
D-AMS 013012	SL15JH07	Tufa, Ten-Mile Ridge	12072	47	13916	13770	14072	**13.921**	0.151
D-AMS 013013	SL15BM04	Tufa, Ten-Mile Ridge	25667	110	29819	29448	30270	**29.859**	0.411
D-AMS 013014	SLT1-2C-1	Tufa, E of Klippel Point	12476	42	14663	14288	14998	**14.643**	0.355
D-AMS 013015	SLT3-1B	Tufa, Carlon Rd Quarry	12533	42	14838	14473	15106	14.790	0.317
CAMS 54469§	RML-1C	Shell, Carlon Rd Quarry	42200	1110	45558	43468	47777	45.623	2.155
CAMS 54470§	RML-BS	Shell, Carlon Rd Quarry	38320	690	42427	41431	43414	42.423	0.992
CAMS 54471§	RML-T	Sheeted tufa, Fremont Pt	35540	490	40133	39012	41207	40.110	1.098
I-11, 177#	*unknown*	Shell, Ten-Mile Ridge	17500	300	21155	20385	21918	21.152	0.766
I-11, 136#	*unknown*	Shell, Carlon Rd Quarry	22080	660	24828	25046	27636	26.341	1.295
D-AMS 16778	SL15AE07	Tufa, Ten-Mile Ridge	36578	214	41225	40705	41674	40.965	0.484
D-AMS 16779	SL15JH04	Tufa, N end of SL	12310	37	14240	14074	14541	14.157	0.233
D-AMS 16780	SL15BM03	Tufa, N end of SL	12041	35	13883	13763	14020	13.823	0.128
D-AMS 16781	SL15JH08	Tufa, Ten-Mile Ridge	19480	53	23473	23184	23689	23.328	0.252
D-AMS 16781	SL15JH07	Tufa, Ten-Mile Ridge	11712	41	13522	13438	13605	13.480	0.083
D-AMS 16783	SL15JH06	Tufa, Ten-Mile Ridge	25655	80	29787	29466	30204	29.626	0.369
D-AMS 16784	SL15AE04	Tufa, Flatiron Point	25291	82	29348	29053	29617	29.200	0.282
D-AMS 16785	SL15BM04	Tufa, Five-mile butte	17663	53	21370	21102	21608	21.236	0.253
D-AMS 16786	SL15AE05	Tufa, Flatiron Point	12273	37	14179	14034	14403	14.106	0.184
D-AMS 16787	SLT1-2C-1	Tufa, NW end of SL	12288	37	14202	14054	14460	14.128	0.203
D-AMS 16788	SL15AE09	Tufa, Ten-Mile Ridge	43390	321	46538	45806	47372	34.929	0.783

* Where italicized, latitude and longitude are estimated based on descriptions of map locations.
† Sample from Freidel, 2001
§ Sample from Robert Langridge, unpublished data
# Sample from Allison, 1982
Bold calibrated ages and elevations are used in the hydrograph

TABLE 3. MOMENT MAGNITUDE CALCULATIONS, FAULTS IN SUMMER LAKE BASIN

Fault**	MD[#] (m)	Hemphill-Haley and Weldon (1999) Max M_w	Min M_w	Range M_w	Wells and Coppersmith (1994) SRL	Range M
Winter Ridge (4 profiles)						
100% of fault *(UVCDS[*] = 0.36, MVCDS[†] = 1.05, LVCDS[§] = 1.69)*	2.34	7.614	7.063	7.1–7.6	30 km	6.4–7.2
75% of fault *(UVCDS[*] = 0.5, MVCDS[†] = 0.88, LVCDS[§] = 1.76)*	2.34	7.599	7.000	7.0–7.6	40 km	6.5–7.4
Slide Mountain (4 profiles)						
100% of fault *(UVCDS[*] = 0.36, MVCDS[†] = 1.05, LVCDS[§] = 1.69)*	1.96	7.551	7.000	7.0–7.6	15 km	6.0–6.8
75% of fault *(UVCDS[*] = 0.5, MVCDS[†] = 0.88, LVCDS[§] = 1.76)*	1.96	7.371	6.923	6.9–7.4	20 km	7.1–7.9
Winter Ridge + Slide Mountain						
100% of fault *(UVCDS[*] = 0.52, MVCDS[†] = 1.03, LVCDS[§] = 1.46)*	2.14	7.444	7.077	7.1–7.4	45 km	6.6–7.5
75% of fault *(UVCDS[*] = 0.66, MVCDS[†] = 0.85, LVCDS[§] = 1.62)*	2.14	7.291	6.971	**7.0–7.3**	60 km	6.8–7.6
Thousand Springs/Summer Lake (9 profiles)						
75% of fault *(UVCDS[*] = 0.68, MVCDS[†] = 0.83, LVCDS[§] = 1.6)*	2.0	7.248	6.943	6.9–7.2	9 km	5.7–6.5
50% of fault *(UVCDS[*] = 0.55, MVCDS[†] = 0.69, LVCDS[§] = 1.76)*	2.0	7.258	6.843	**6.8–7.3**	18 km	6.1–6.9
25% of fault *(UVCDS[*] = 0.28, MVCDS[†] = 0.69, LVCDS[§] = 2.09)*	2.0	7.498	6.782	6.8–7.5	30 km	6.4–7.2

[*] Upper value combined displacement statistics (Hemphill-Haley and Weldon, 1999)

[†] Mode value combined displacement statistics (Hemphill-Haley and Weldon, 1999)

[§] Lower value combined displacement statistics (Hemphill-Haley and Weldon, 1999)

[#] Mean displacement

** Assumed dips of 60° for all displacement calculations

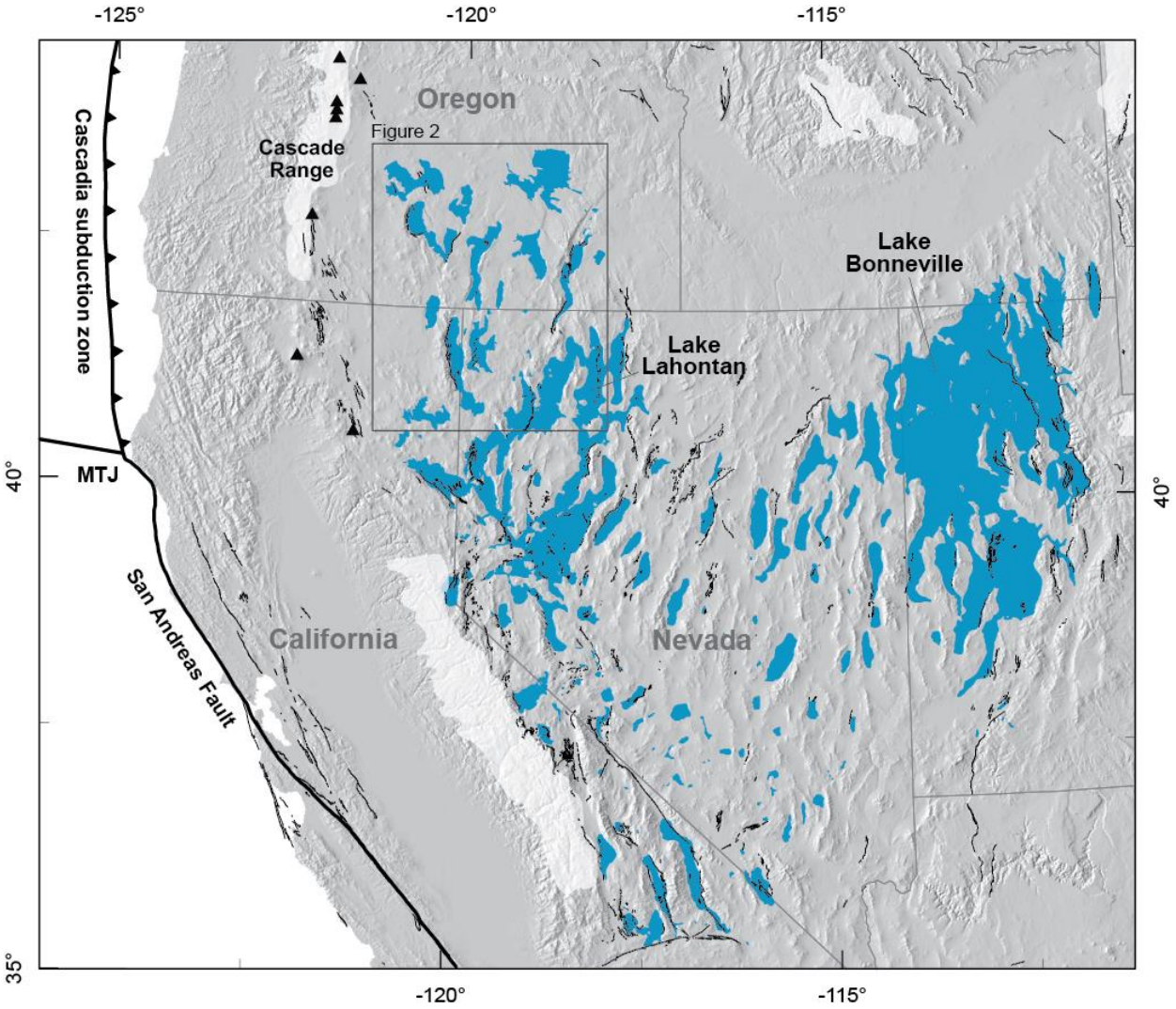

Figure 1. Map showing plate boundaries, Quaternary faults that have ruptured since 15 ka (U.S. Geological Survey, 2006), extent of ice sheets during the Last Glacial Maximum in white, and the maximum extent of pluvial lakes in blue. Triangles indicate active volcanoes in the Cascades arc. MTJ—Mendocino Triple Junction. Inset box indicates area shown in Figure 2.

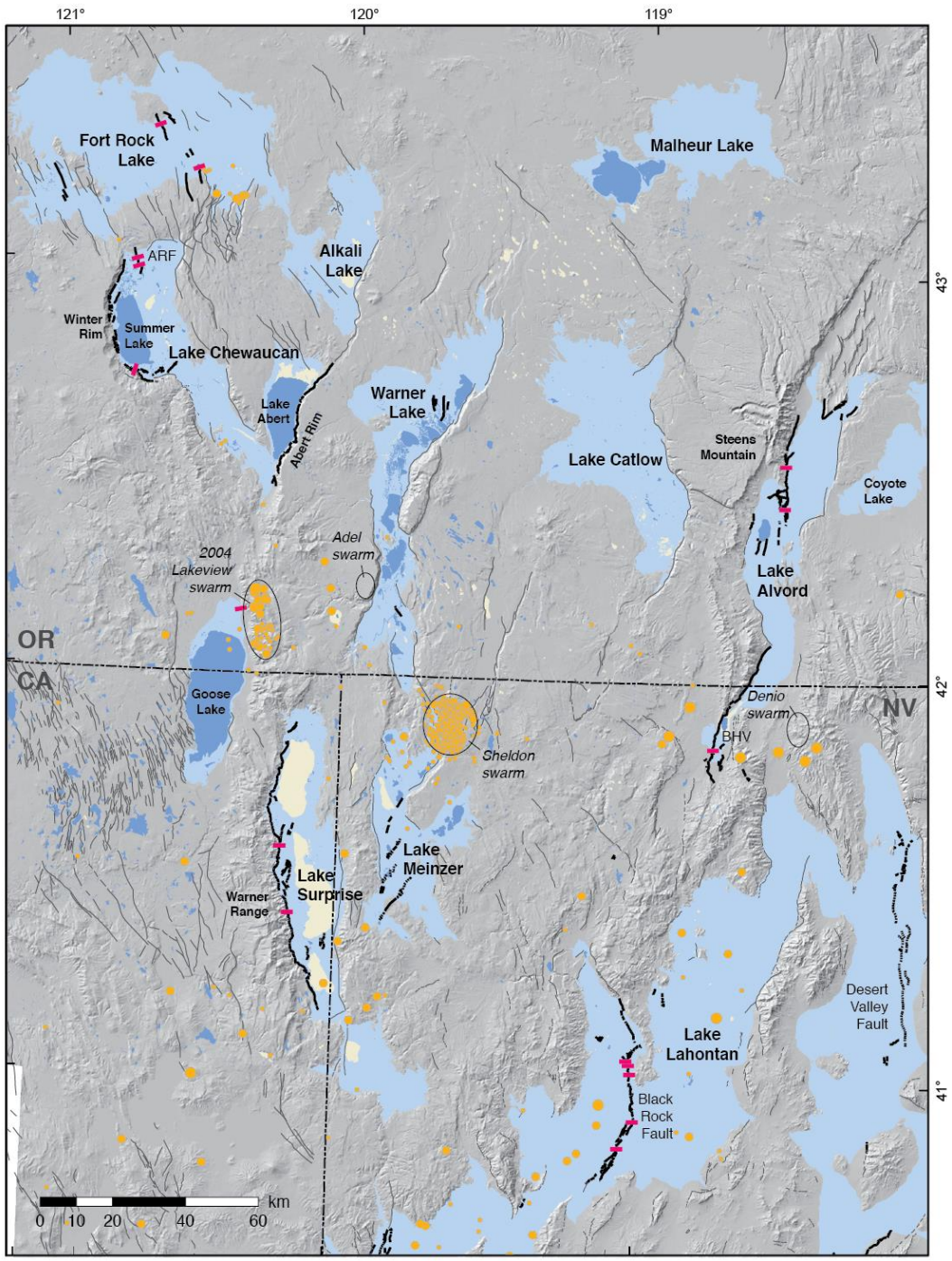

Figure 2. Map of the northwestern Basin and Range (NWBR) showing faults active in the last 15 ka (U.S. Geological Survey and Nevada Bureau of Mines and Geology, 2006). Pink lines indicate locations of paleoseismic trenches (see text for discussion). Approximate maximum extents of pluvial lakes are shown in light blue, derived in ArcGIS from the published highstands (see text for sources for individual lakes) and 10-m DEMs (Gesch, 2007); modern lakes and playas shown in darker blue and tan, respectively. Orange circles indicate earthquakes >M_w2 from 1974 to 2015 (ANSS, 2009); location of 1968 Adel swarm from Schaff (1976); the location of the 1973 Denio swarm from Richins (1974). ARF—Ana River Fault; BHV—Bog Hot Valley.

Figure 3. Map of the Winter Rim fault system and Summer Lake Basin in context of the surrounding region. Highstands of Lake Chewaucan and Fort Rock Lake are from Allison (1982). Locations of cores from Kuehn and Negrini (2010). Radiocarbon geochronology samples from a variety of sources, compiled in Table 2 (for Summer Lake basin).

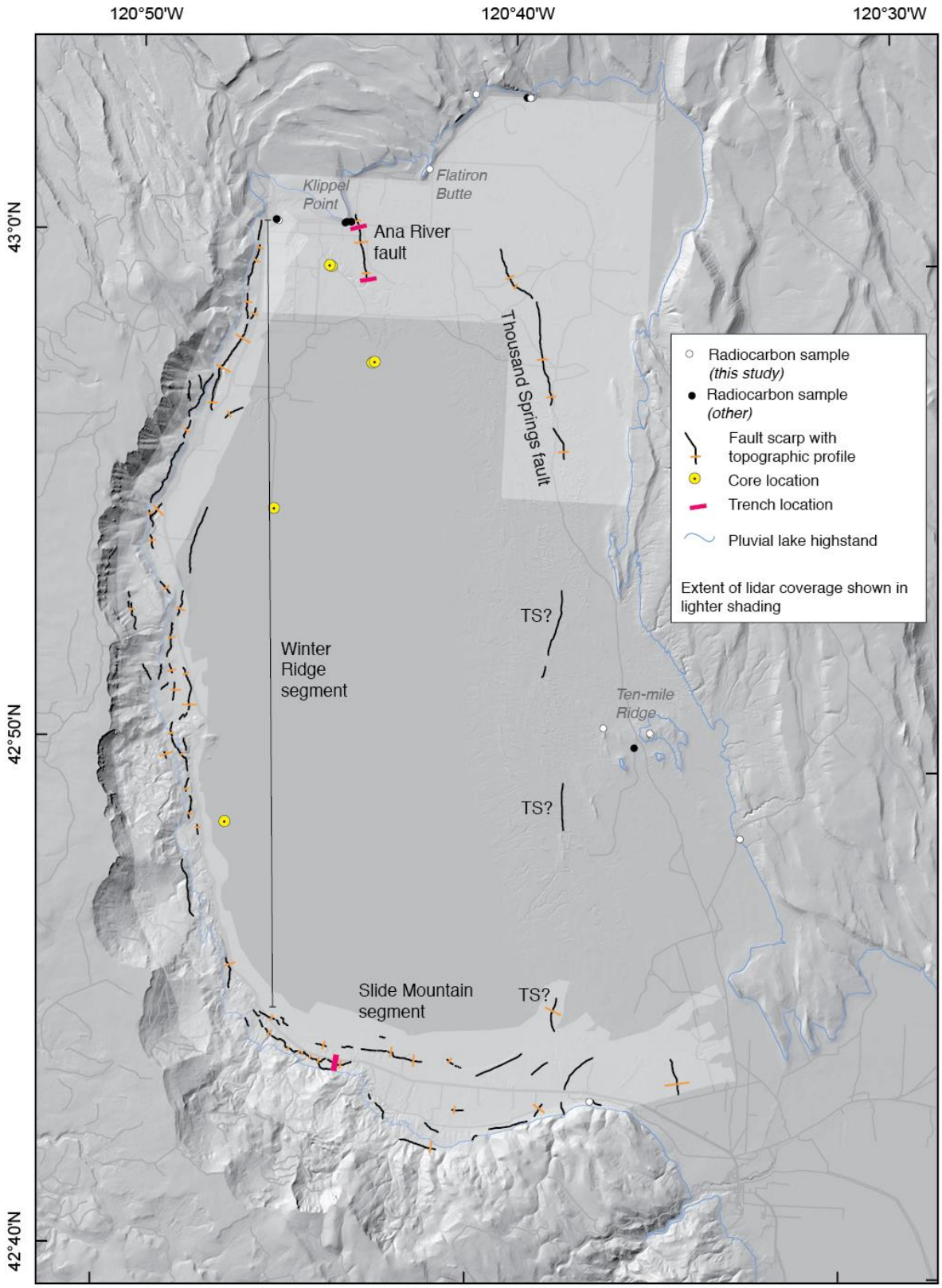

Figure 4. Map of the Winter Rim fault system and Summer Lake Basin showing mapped fault scarps, extent of lidar data coverage, locations of topographic profiles used in magnitude calculations and Figures 5 and 6, and the possible extent of the Thousand Springs fault (indicated by TS?).

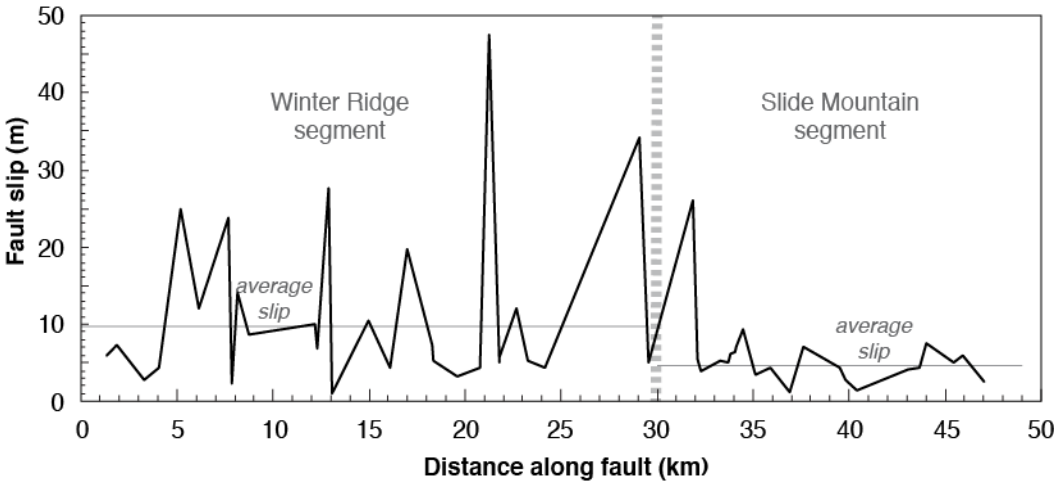

Figure 5. Graph showing fault slip calculated from surface offsets along fault scarps along the length of the Winter Rim fault system. The wide dashed line represents the change in orientation that marks the transition from the Winter Ridge segment (with a strike of approximately 350°) to the Slide Mountain segment (with a strike of approximately 270°).

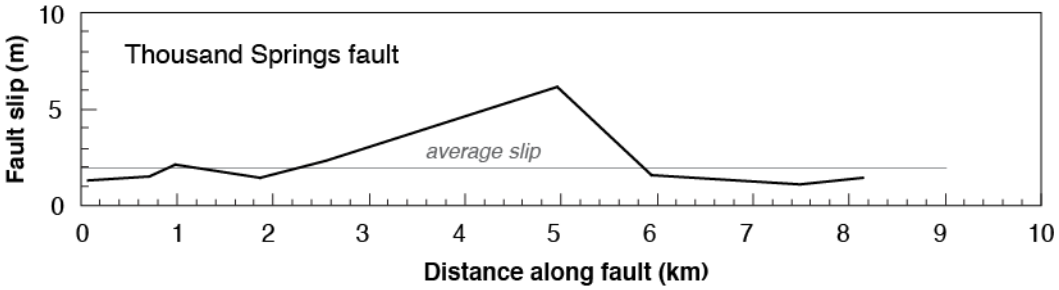

Figure 6. Graph showing fault slip calculated from surface offsets along fault scarps along the length of the northernmost portion of the Thousand Springs/Summer Lake fault.

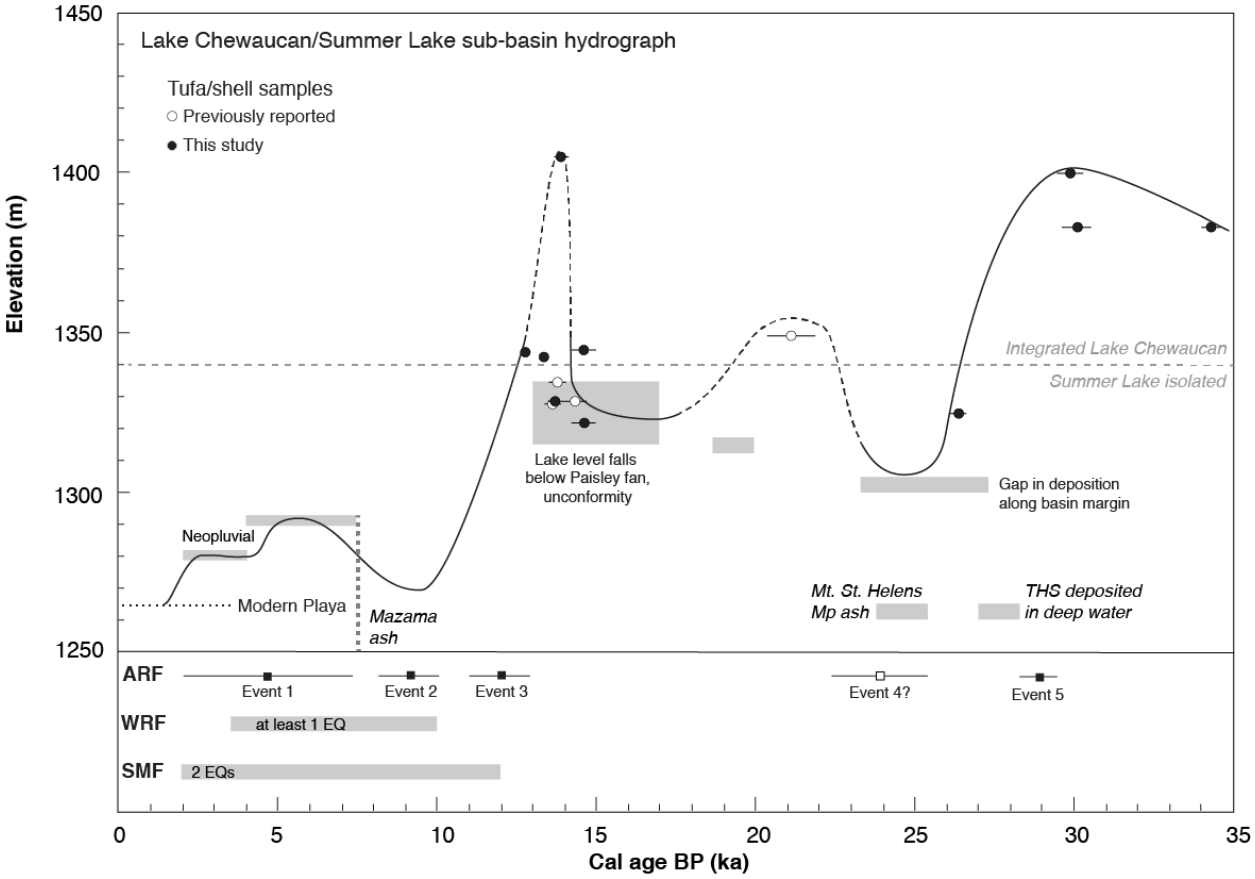

Figure 7. Combined hydrograph and earthquake record for Summer Lake and the Ana River fault (ARF), Slide Mountain fault (SMF), and Winter Rim fault (WRF). Earthquakes and age constraints from the ARF are presented in this study; constraints from the SMF and WRF are from Pezzopane (1993). The gap in deposition indicating low lake level from Cohen et al. (2000), Negrini et al. (2000), and Negrini and Davis (1992). Exposure of Paisley fan from and Jenkins et al. (2012) and Allison (1982). Age of Mazama ash from Zdanowicz et al. (1999); Mt. St. Helens Mp ash age from Mullineaux (1986).

REFERENCES CITED

Adams, K. D., and Wesnousky, S. G., 1998, Shoreline processes and the age of the Lake Lahontan highstand in the Jessup embayment, Nevada: Geological Society of America Bulletin, v. 110, no. 10, p. 1318-1332. doi: 10.1130/0016-7606(1998)110<1318:spatao>2.3.co;2

-, 1982, Geology of pluvial Lake Chewaucan, Lake County, Oregon: Corvallis, Oregon, Oregon State University Press, Studies in Geology, v. 11, 79 p.

Amos, C. B., Audet, P., Hammond, W. C., Burgmann, R., Johanson, I. A., and Blewitt, G., 2014, Uplift and seismicity driven by groundwater depletion in central California: Nature, v. 509, no. 7501, p. 483-486. doi: 10.1038/nature13275

Anderson, E. M., 1951, The dynamics of faulting and dyke formation with applications to Britain, London, England, Hafner Publishing Company.

ANSS, 2009, Advanced National Seismic System Catalog, Northern California Earthquake Data Center.

Badger, T. C., and Watters, R. J., 2004, Gigantic seismogenic landslides of Summer Lake basin, south-central Oregon: Geological Society of America Bulletin, v. 116, no. 5-6, p. 687-697. doi: 10.1130/b25333.1

Berg, J. W. J., and Baker, C. D., 1963, Oregon earthquakes, 1841 through 1958: Bulletin of the Seismological Society of America, v. 53, no. 1, p. 95-108.

Cohen, A., Palacios-Fest, M., Negrini, R., Wigand, P., and Erbes, D., 2000, A paleoclimate record for the past 250,000 years from Summer Lake, Oregon, USA: II. Sedimentology, paleontology and geochemistry: Journal of Paleolimnology, v. 24, no. 2, p. 151-182. doi: 10.1023/a:1008165326401

Davis, J. O., 1985, Correlation of late Quaternary tephra layers in a long pluvial sequence near Summer Lake, Oregon: Quaternary Research, v. 23, no. 1, p. 38-53.

DePolo, C. M., Clark, D. G., Slemmons, D. B., and Ramelli, A. R., 1991, Historical surface faulting in the Basin and Range province, western North America: implications for fault segmentation: Journal of Structural Geology, v. 13, no. 2, p. 123-136.

DirectAMS, 2015, Prices and Services, Volume 2016.

Egger, A. E., Ibarra, D. E., Weldon, R., Langridge, R. M., Marion, B., and Hall, J., *in review*, The influence of pluvial lake cycles on earthquake recurrence in the northwestern Basin and Range, USA; GSA Special Papers, Scott Starrat, Editor

Egger, A. E., and Miller, E. L., 2011, Evolution of the northwestern margin of the Basin and Range: The geology and extensional history of the Warner Range and environs, northeastern California: Geosphere, v. 7, no. 3, p. 756-773. doi: 10.1130/ges00620.1

Felton, A., Jewell, P. W., Chan, M., and Currey, D., 2006, Controls of Tufa Development in Pleistocene Lake Bonneville, Utah: The Journal of Geology, v. 114, no. 3, p. 377-389. doi: 10.1086/501218

Freidel, D. E., 1993, Chronology and climatic controls of late Quaternary lake-level fluctuations in Chewaucan, Fort Rock, and Alkali basins, south-central Oregon [Ph.D. thesis]: University of Oregon, 125 p.

Friedrich, A. M., Wernicke, B. P., Niemi, N. A., Bennett, R. A., and Davis, J. L., 2003, Comparison of geodetic and geologic data from the Wasatch region, Utah, and implications for the spectral character of Earth deformation at periods of 10 to 10 million years: Journal of Geophysical Research: Solid Earth, v. 108, no. B4, p. n/a-n/a. doi: 10.1029/2001JB000682

Gesch, D. B., 2007, The National Elevation Dataset, *in* Maune, D., ed., Digital Elevation Model Technologies and Applications: The DEM Users Manual: Bethesda, Maryland, American Society for Photogrammetry and Remote Sensing, p. 99-118.

Hemphill-Haley, M. A., and Weldon, R. J., 1999, Estimating prehistoric earthquake magnitude from point measurements of surface rupture: Bulletin of the Seismological Society of America, v. 89, no. 5, p. 1264-1279.

Hudson, A., Quade, J., Ali, G. A. H., Boyle, D., Bassett, S., and Huntington, K., 2015, Combining ^{14}C/U-Th Series Geochronology and Stable/Clumped Isotope Geochemistry of MIS 2 Lake Tufas of Lake Chewaucan, Oregon, USA to Reconstruct Deglacial Climate in the Pacific Northwest: Eos (Transactions, American Geophysical Union), Abstract PP12A-04.

Ibarra, D. E., Egger, A. E., Weaver, K. L., Harris, C. R., and Maher, K., 2014, Rise and fall of late Pleistocene pluvial lakes in response to reduced evaporation and precipitation: Evidence from Lake Surprise, California: Geological Society of America Bulletin, v. B31014.1, 30 p. doi: 10.1130/B31014.1

Kreemer, C., Hammond, W. C., Blewitt, G., Holland, A. A., and Bennett, R. A., 2012, A Geodetic Strain Rate Model for the Pacific-North American Plate Boundary, Western United States, Volume M178: Reno, NV, Nevada Bureau of Mines and Geology, 1 sheet.

Kuehn, S. C., and Negrini, R. M., 2010, A 250 k.y. record of Cascade arc pyroclastic volcanism from late Pleistocene lacustrine sediments near Summer Lake, Oregon, USA: Geosphere, v. 6, no. 4, p. 397-429. doi: 10.1130/ges00515.1

Kurth, G., Phillips, F. M., Reheis, M. C., Redwine, J. L., and Paces, J. B., 2011, Cosmogenic nuclide and uranium-series dating of old, high shorelines in the western Great Basin,

USA: Geological Society of America Bulletin, v. 123, no. 3-4, p. 744-768. doi: 10.1130/b30010.1

Langridge, R. M., 1998, Paleoseismic deformation in behind-arc lacustrine settings: Acambay, Mexico and Ana River [Ph.D. thesis]: University of Oregon, 188 p.

Langridge, R. M., Pezzopane, S. K., and Weldon, R. J., 2001, Slip rate, recurrence intervals and paleoearthquakes for the Ana River Fault, central Oregon, *in* Negrini, R., Pezzopane, S. K., and Badger, T. C., eds., Quaternary Studies near Summer Lake, Oregon, Friends of the Pleistocene, p. 126.

Licciardi, J. M., 2001, Chronology of latest Pleistocene lake-level fluctuations in the pluvial Lake Chewaucan basin, Oregon, USA: Journal of Quarternary Science, v. 16, no. 6, p. 545-553. doi: 10.1002/jqs.619

Llenos, A. L., McGuire, J. J., and Ogata, Y., 2009, Modeling seismic swarms triggered by aseismic transients: Earth and Planetary Science Letters, v. 281, no. 1–2, p. 59-69. doi: http://dx.doi.org/10.1016/j.epsl.2009.02.011

Lohman, R. B., and McGuire, J. J., 2007, Earthquake swarms driven by aseismic creep in the Salton Trough, California: Journal of Geophysical Research: Solid Earth, v. 112, no. B4, p. 2156-2202. doi: 10.1029/2006JB004596

Mifflin, M. D., and Wheat, M. M., 1979, Pluvial Lakes and Estimated Pluvial Climates of Nevada: Reno, Nevada, Nevada Bureau of Mines and Geology.

Mogi, K., 1963, Some Discussions on Aftershocks, Foreshocks, and Earthquake Swarms—the Fracture of a Semi-infinite Body Caused by an Inner Stress Origin and Its Relation to the Earthquake Penomena: Bulletin of the Earthquake Research Institute, v. 41, p. 615-668.

Mullineaux, D. R., 1986, Summary of pre-1980 tephra-fall deposits erupted from Mount St. Helens, Washington State, USA: Bulletin of Volcanology, v. 48, no. 1, p. 17-26. doi: 10.1007/BF01073510

Negrini, R., Erbes, D., Faber, K., Herrera, A., Roberts, A., Cohen, A., Wigand, P., and Foit, F., 2000, A paleoclimate record for the past 250,000 years from Summer Lake, Oregon, USA. 1. chronology and magnetic proxies for lake level: Journal of Paleolimnology, v. 24, no. 2, p. 125-149. doi: 10.1023/a:1008144025492

Negrini, R. M., and Davis, J. O., 1992, Dating late Pleistocene pluvial events and tephras by correlating paleomagnetic secular variation records from the western Great Basin: Quaternary Research, v. 38, no. 1, p. 46-59. doi: http://dx.doi.org/10.1016/0033-5894(92)90029-I

Nelson, S. T., Wood, M. J., Mayo, A. L., Tingey, D. G., and Eggett, D., 2005, Shoreline tufa and tufaglomerate from Pleistocene Lake Bonneville, Utah, USA: stable isotopic and mineralogical records of lake conditions, processes, and climate: Journal of Quaternary Science, v. 20, no. 1, p. 3-19. doi: 10.1002/jqs.889

Personius, S. F., Dart, R. L., Bradley, L.-A., and Haller, K. M., 2003, Map and data for Quaternary faults and folds in Oregon: U.S. Geological Survey Open-File Report 2003-95.

Pezzopane, S. K., 1993, Active faults and earthquake ground motions in Oregon [Ph.D. thesis]: University of Oregon, 250 p.

-, 2001, Pluvial Lake Chewaucan shoreline elevations, *in* Negrini, R., Pezzopane, S. K., and Badger, T. C., eds., Quaternary Studies near Summer Lake, Oregon: Paisley, OR, Friends of the Pleistocene, 4 p.

Pezzopane, S. K., and Weldon, R. J., II, 1993, Tectonic role of active faulting in central Oregon: Tectonics, v. 12, no. 5, p. 1140-1169. doi: 10.1029/92tc02950

Reheis, M., 1999a, Extent of Pleistocene Lakes in the Western Great Basin: U.S. Geological Survey Miscellaneous Field Studies Map 2323.

-, 1999b, Highest Pluvial-Lake Shorelines and Pleistocene Climate of the Western Great Basin: Quaternary Research, v. 52, no. 2, p. 196-205. doi: 10.1006/qres.1999.2064

Reheis, M. C., Adams, K. D., Oviatt, C. G., and Bacon, S. N., 2014, Pluvial lakes in the Great Basin of the western United States—A view from the outcrop: Quaternary Science Reviews, v. 97, p. 33-57. doi: http://dx.doi.org/10.1016/j.quascirev.2014.04.012

Reimer, P. J., Bard, E., Bayliss, A., Beck, J. W., Blackwell, P. G., Ramsey, C. B., Buck, C. E., Cheng, H., Edwards, R. L., Friedrich, M., Grootes, P. M., Guilderson, T. P., Haflidason, H., Hajdas, I., Hatté, C., Heaton, T. J., Hoffmann, D. L., Hogg, A. G., Hughen, K. A., Kaiser, K. F., Kromer, B., Manning, S. W., Niu, M., Reimer, R. W., Richards, D. A., Scott, E. M., Southon, J. R., Staff, R. A., Turney, C. S. M., and Plicht, J. v. d., 2013, IntCal13 and Marine13 Radiocarbon Age Calibration Curves 0–50,000 Years cal BP: Radiocarbon, v. 55, no. 4, p. 19. doi: 10.2458/azu_js_rc.55.16947

Richardson, E., Newton, M., Rubio, E., and McGuire, J. J., Searching for earthquake swarms and aseismic deformation in the Western U.S: Eos (Transactions, American Geophysical Union), Abstract S33B-2098.

Richins, W. D., 1974, Earthquake swarm near Denio, Nevada, February to April, 1973 [M.S. thesis]: University of Nevada, Reno, 57 p.

Scarberry, K. C., Meigs, A. J., and Grunder, A. L., 2010, Faulting in a propagating continental rift: Insight from the late Miocene structural development of the Abert Rim fault,

southern Oregon, USA: Tectonophysics, v. 488, no. 1-4, p. 71-86. doi: 10.1016/j.tecto.2009.09.025

Schaff, S. C., 1976, The 1968 Adel, Oregon, earthquake swarm [M.S. thesis]: University of Nevada, Reno, 63 p.

Smith, R. B., and Sbar, M. L., 1974, Contemporary Tectonics and Seismicity of the Western United States with Emphasis on the Intermountain Seismic Belt: Geological Society of America Bulletin, v. 85, no. 8, p. 1205-1218. doi: 10.1130/0016-7606(1974)85<1205:ctasot>2.0.co;2

Strickley, D., 2014, Controls on fault geometry during early stages of extension in the Larkspur Hills, northwest Basin and Range [M.S. thesis]: Central Washington University.

Stuiver, M., and Reimer, P. J., 1986-2015, Calib 7.1.

Surpless, B., and Kroeger, G., 2015, The unusual temporal and spatial slip history of the Wassuk Range normal fault, western Nevada (USA): Implications for seismic hazard and Walker Lane deformation: Geological Society of America Bulletin, v. 127, no. 5-6, p. 737-758. doi: 10.1130/b31159.1

Treerotchananon, A., 2009, Extension between major faults, central Oregon Basin and Range [M.S. thesis]: University of Oregon, 71 p.

Trench, D., Meigs, A., and Grunder, A., 2012, Termination of the northwestern Basin and Range province into a clockwise rotating region of transtension and volcanism, southeast Oregon: Journal of Structural Geology, v. 39, p. 52-65. doi: 10.1016/j.jsg.2012.03.007

U.S. Geological Survey, 2006, Quaternary fault and fold database for the United States.

U.S. Geological Survey and Nevada Bureau of Mines and Geology, 2006, Quaternary fault and fold database for the United States.

Uhrhammer, R. A., 1991, Northern California seismicity, *in* Slemmons, D. B., Engdahl, E. R., Zoback, M. D., and Blackwell, D. D., eds., Neotectonics of North America, Volume 1: Boulder, CO, Geological Society of America, p. 99-106.

Vidale, J. E., and Shearer, P. M., 2006, A survey of 71 earthquake bursts across southern California: Exploring the role of pore fluid pressure fluctuations and aseismic slip as drivers: Journal of Geophysical Research: Solid Earth, v. 111, no. B5. doi: 10.1029/2005JB004034

Wallace, R. E., 1987, Grouping and migration of surface faulting and variations in slip rates on faults in the Great Basin province: Bulletin of the Seismological Society of America, v. 77, no. 3, p. 868-876.

Weaver, C. S., and Hill, D. P., 1978, Earthquake swarms and local crustal spreading along major strike-slip faults in California: Pure and Applied Geophysics, v. 117, no. 1, p. 51-64. doi: 10.1007/bf00879733

Weldon, R. J., Fletcher, D. K., Weldon, E. M., Scharer, K. M., and McCrory, P. A., 2003, An update of Quaternary faults of central and eastern Oregon: U.S. Geological Survey Open-File Report 2002-301.

Weldon, R. J., Langridge, R. M., Pezzopane, S. K., and Weldon, E., 2009, An earthquake cluster followed the drying of Pleistocene Lake Chewaucan, central Oregon Basin and Range: Geological Society of America Abstracts with Programs, v. 41, no. 7, p. 456.

Wells, D. L. and Coppersmith, K. J., 1994, New empirical relationships among magnitude, rupture length, rupture width, rupture area, and surface displacement: Bulletin of the Seismological Society of America, v. 84, no. 4, p. 974-1002.

Wolterbeek, M., 2015, Earthquake activity in far northwest Nevada continues, Nevada Today, University of Nevada, Reno.

Zdanowicz, C. M., Zielinski, G. A., and Germani, M. S., 1999, Mount Mazama eruption: Calendrical age verified and atmospheric impact assessed: Geology, v. 27, no. 7, p. 621-624. doi: 10.1130/0091-7613(1999)027<0621:mmecav>2.3.co;2